



Analysis and fit of the high-resolution spectrum of the $\tilde{A}^1A_u-\tilde{X}^1A_g$ LIF spectrum of the two-equivalent-top molecule biacetyl

Chen-Lin Liu^a, Cheng-Liang Huang^b, Chi-Kung Ni^a, Nobukimi Ohashi^c, Jon T. Hougen^{d,*}

^a Institute of Atomic and Molecular Sciences, Academia Sinica, Taipei 106, P.O. Box 23-166, Taiwan

^b Department of Applied Chemistry, National Chiayi University, Chiayi, Taiwan

^c Kanazawa University, Kanazawa 920-1192, Japan

^d Optical Technology Division, National Institute of Standards and Technology, Gaithersburg, MD 20899-8441, USA

ARTICLE INFO

Article history:

Received 26 February 2009

In revised form 13 April 2009

Available online 23 April 2009

Keywords:

Biacetyl

Internal rotation

Least-squares fit

Rotational analysis

Torsion-rotation levels

Two methyl tops

ABSTRACT

The jet-cooled laser-induced visible fluorescence excitation spectrum of the $\tilde{A}^1A_u(S_1)-\tilde{X}^1A_g(S_0)$ transition in biacetyl ($\text{CH}_3\text{-C(=O)-C(=O)-CH}_3$) exhibits a long progression in the torsional vibrations of the two equivalent methyl tops in this molecule, whose structure has previously been described and qualitatively understood using local mode ideas applied to the two equivalent methyl rotor torsions together with the G_{36} symmetry species $A_1, A_2, A_3, A_4, E_1, E_2, E_3, E_4,$ and G . In the present rotational analysis, we have assigned a G_{36} symmetry species, two local-mode torsional quantum numbers, and the usual three asymmetric rotor quantum numbers J_{KaKc} to the upper and lower torsion-rotation levels involved in the observed transitions, relying heavily on comparison of quantum-beat patterns to determine transitions with a common upper state. These torsion-rotation transitions were then globally fit using a two-equivalent-top computer program, which was written in the principal axis system of the molecule and which uses a free-rotor basis set for each top, a symmetric-top basis set for the rotational functions, and a single-step diagonalization procedure. We can fit 411 lines involving 16 torsional sublevels from states with zero to three quanta of torsional excitation in the excited electronic state, using 24 parameters to obtain a standard deviation of 0.0045 cm^{-1} , which is quite satisfactory, but inclusion in the fit of 440 transitions from all 17 rotationally assigned torsional levels increases the standard deviation by some 25%. The present fit gives a value of $V_3 = 238\text{ cm}^{-1}$ for the threefold barrier height in the excited electronic state, in reasonable agreement with earlier studies.

© 2009 Elsevier Inc. All rights reserved.

1. Introduction

This is the third in a series of papers on the laser-induced fluorescence (LIF) excitation spectrum of the $\tilde{A}^1A_u(S_1)-\tilde{X}^1A_g(S_0)$ electronic transition of biacetyl ($\text{CH}_3\text{-C(=O)-C(=O)-CH}_3$). In the first paper [1] experimental details and rotational analyses using an asymmetric-rotor Hamiltonian for the seven lowest-lying bands in the upper state torsional progression were reported. In the second paper [2], a quantitative fit of 15 torsional band centers in the $\tilde{A}^1A_u(S_1)$ upper electronic state to a two-equivalent-rotor torsional Hamiltonian was carried out, and the positions of the levels were discussed qualitatively in terms of a local-mode model. The reader is referred to those two papers for a more extensive introduction to the problem and for references to earlier work.

This paper is concerned with a global least-squares fit of rotational energy levels belonging to various torsional sublevels in the $\tilde{A}^1A_u(S_1)$ electronic state, using a two-equivalent-top

torsion-rotation Hamiltonian based on the G_{36} permutation-inversion group. This G_{36} Hamiltonian is quite similar to the two-inequivalent-top Hamiltonian based on the G_{18} permutation-inversion group used previously to carry out a rotational fit to the microwave spectrum of the closely related molecule *N*-methylacetamide ($\text{CH}_3\text{-C(=O)-N(-H)-CH}_3$) [3].

Our global fits have been relatively successful, in the sense that overall standard deviations of the fits are within a factor of two or three of the estimated experimental measurement uncertainty. Nevertheless, a fit to 415 rotational transitions from 16 torsional sublevels using 24 parameters (different from the fit cited in the abstract), gives a root-mean-square (rms) residual of 0.0049 cm^{-1} , while attempts to fit 440 rotational transitions from all 17 torsional sublevels having rotational assignments lead to a significant increase in the rms residual to 0.0057 cm^{-1} , indicating that some unexplained difficulties remain.

The rest of this paper contains the following parts. We briefly review the G_{36} group theory needed to classify torsion-rotation states in this molecule in Section 2, and discuss the form of the torsion-rotation Hamiltonian in Section 3. We discuss the data set in Section 4 and the results of our least-squares fits in Section 5.

* Corresponding author. Fax: +1 301 975 2950.

E-mail address: jon.hougen@nist.gov (J.T. Hougen).

2. Group theory

Biacetyl has C_{2h} point-group symmetry at equilibrium, but, as discussed by Senent et al. [4], it belongs to the permutation–inversion (PI) group G_{36} when internal rotations of the two methyl groups are considered. We use here the atom numbering scheme shown in Fig. 1 and the species notation and character table given by Nelson and Klemperer in their study of the ammonia dimer [5], which can also be found in our first paper in this series [1].

The precise relations between the G_{36} PI operations and the transformations of variables in the torsion–rotation wavefunctions are determined here, as usual, by first setting up an algebraic relation between the laboratory-fixed coordinates and a somewhat idealized set of molecule-fixed coordinates that preserve the essential symmetry of the problem:

$$\mathbf{R}_i = \mathbf{R} + S^{-1}(\chi, \theta, \phi) S^{-1}(0, \theta_{\text{PAM}}, 0) \mathbf{a}_i(\alpha_1, \alpha_2), \quad (1)$$

where

$$\begin{aligned} \mathbf{a}_i(\alpha_1, \alpha_2) &= \mathbf{a}_i^0 \quad \text{for } i = a-f \\ \mathbf{a}_i(\alpha_1, \alpha_2) &= [S^{-1}(+\alpha_1, 0, 0)(\mathbf{a}_i^0 - \mathbf{a}_{\text{Ca}}^0) + \mathbf{a}_{\text{Ca}}^0] \quad \text{for } i = 1-3 \\ \mathbf{a}_i(\alpha_1, \alpha_2) &= [S^{-1}(-\alpha_2, 0, 0)(\mathbf{a}_i^0 - \mathbf{a}_{\text{Cb}}^0) + \mathbf{a}_{\text{Cb}}^0] \quad \text{for } i = 4-6 \end{aligned} \quad (2)$$

In Eq. (1), the \mathbf{R}_i on the left represent 3×1 vectors containing laboratory-fixed Cartesian coordinates for the atoms $i = 1-6$ and $a-f$ of the molecule, as labeled in Fig. 1. On the right, \mathbf{R} represents a 3×1 vector containing the laboratory-fixed Cartesian coordinates of the center of mass of the molecule; $S^{-1}(\chi, \theta, \phi)$ represents the 3×3 direction cosine matrix between the laboratory-fixed and molecule-fixed axes, as defined using the Euler angle conventions of [6]; the $\mathbf{a}_i(\alpha_1, \alpha_2)$ represent 3×1 vectors containing the molecule-fixed Cartesian coordinates of the atoms, defined as functions of the internal rotation angles α_1 and α_2 in Eq. (2); and the constant matrix $S^{-1}(0, \theta_{\text{PAM}}, 0)$ rotates the whole molecule about the y axis into a “torsion–rotation principal axis system” (see Section 5). In Eq. (2), the constant vectors \mathbf{a}_i^0 represent the set of “initial atom positions” given in Table 1, where the C_3 axes of the methyl tops are parallel to the molecule-fixed z axis and point towards the C_c or C_d carbon atoms to which they are bonded; the matrices $S^{-1}(+\alpha_1, 0, 0)$ and $S^{-1}(-\alpha_2, 0, 0)$ carry out the internal rotation of

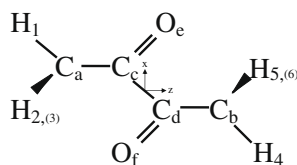


Fig. 1. Atom numbering scheme for biacetyl adopted in this work. All atoms lie in the plane of the paper, except for H_2 and H_5 , which are above the plane, and H_3 and H_6 , which are below the plane of the paper and completely eclipsed by H_2 and H_5 , respectively, in the view shown in this figure. The x and z axes chosen are shown by arrows.

Table 1
Schematic values for the coordinates^a \mathbf{a}_i^0 used in the idealized structure of Eq. (2).

Atom ^b	a_x^0	a_y^0	a_z^0	Atom ^b	a_x^0	a_y^0	a_z^0
C_a	$+x_a$	0	$-z_a$	H_1	$+x_a + x_1$	0	$-z_1$
C_c	$+x_a$	0	$-z_c$	H_2	$+x_a - x_1/2$	$+x_1\sqrt{3}/2$	$-z_1$
O_e	$+x_e$	0	$+z_e$	H_3	$+x_a - x_1/2$	$-x_1\sqrt{3}/2$	$-z_1$

^a The quantities x_a, x_e, x_1 and z_a, z_c, z_e, z_1 are all taken to be positive.

^b Because of the center of symmetry in biacetyl, $\mathbf{a}_i^0 = -\mathbf{a}_j^0$ for the atom pairs $(i, j) = (1, 4), (2, 6), (3, 5), (a, b), (c, d),$ and (e, f) , using the atom labels shown in Fig. 1.

Table 2

Transformation properties of the molecule-fixed coordinates in Eqs. (1) and (2) corresponding to the indicated permutation–inversion (PI) operations^a of the G_{36} group with the atom numbering in Fig. 1.

PI operation ^a	c-o-m ^b	Euler angles ^c	Torsional angles ^d	
E	$+\mathbf{R}$	χ, θ, ϕ	α_1	α_2
$A = (123)$	$+\mathbf{R}$	χ, θ, ϕ	$\alpha_1 + 2\pi/3$	α_2
$B = (456)$	$+\mathbf{R}$	χ, θ, ϕ	α_1	$\alpha_2 + 2\pi/3$
$C = (14)(25)(36)(ab)(cd)(ef)$	$+\mathbf{R}$	$\pi - \chi, \pi - \theta, \pi + \phi$	α_2	α_1
$D = (23)(56)^*$	$-\mathbf{R}$	$\pi - \chi, \pi - \theta, \pi + \phi$	$-\alpha_1$	$-\alpha_2$

^a The operations A, B, C, D are generators for G_{36} .

^b The center-of-mass vector in laboratory-fixed Cartesian coordinates.

^c The rotational variables occurring in the direction cosine matrix $S^{-1}(\chi, \theta, \phi)$ of Eq. (1).

^d Each torsional angle governs the internal rotation of one methyl top (see Eq. (2)).

each methyl group about its C_3 axis, according to its own torsional angle. (We note in passing that constant matrices of the form $S^{-1}(0, \pm\theta_{\text{top}}, 0)$ could be introduced to rotate the two methyl top C_3 axes symmetrically away from the z axis, but this small correction does not change the symmetry properties of the coordinates, so it will not be described here.)

Table 2 gives coordinate transformations for the generators of G_{36} . It can be shown that substitution into the right of Eqs. (1) and (2) of the coordinate changes specified in a given row on the right of Table 2 yields on the left of Eq. (1) the PI transformation given on the left of that row in Table 2. For example, working through the substitutions in the last of Eq. (3) yields the PI operation on the left of Eq. (3):

$$\begin{aligned} &(142635)(ab)(cd)(ef)^* \\ &f(\mathbf{R}_1, \mathbf{R}_2, \mathbf{R}_3, \mathbf{R}_4, \mathbf{R}_5, \mathbf{R}_6, \mathbf{R}_a, \mathbf{R}_b, \mathbf{R}_c, \mathbf{R}_d, \mathbf{R}_e, \mathbf{R}_f) \\ &= f(-\mathbf{R}_4, -\mathbf{R}_6, -\mathbf{R}_5, -\mathbf{R}_2, -\mathbf{R}_1, -\mathbf{R}_3, -\mathbf{R}_b, -\mathbf{R}_a, -\mathbf{R}_d, -\mathbf{R}_c, -\mathbf{R}_f, -\mathbf{R}_e) \\ &= ACD f(\mathbf{R}, \chi, \theta, \phi, \alpha_1, \alpha_2) = f(-\mathbf{R}, \chi, \theta, \phi, -\alpha_2, -\alpha_1 - 2\pi/3) \quad (3) \end{aligned}$$

It can also be seen that the transformation properties in Table 2 are consistent with those described in Eqs. (3)–(5) of our earlier work [2], if we make the identifications α_1, α_2 here = θ_1, θ_2 there. The information in Table 1 of [1] and Table 2 can be used to determine the symmetry species of the torsional basis functions shown in Table 2 of [2] and the rotational basis functions [7] shown in Table 3.

3. Torsion–rotation Hamiltonian operator

The torsion–rotation Hamiltonian operator for the $\tilde{A}^1 A_u(S_1)$ excited electronic state of biacetyl is similar to that used previously for the ground electronic state of N -methylacetamide [3], except that some parameter pairs must be set equal to each other because of the higher symmetry of biacetyl. Also, a number of centrifugal distortion terms that were determinable in the microwave study of [3], but are not determinable in the visible study here, are not explicitly shown in the Hamiltonian of Eq. (4). Similarly, higher-

Table 3

G_{36} symmetry species Γ^a for linear combinations of the symmetric-top rotational basis functions $|K, J, M\rangle$.

Γ	Rotational function	Γ	Rotational function
A_1	$ K=0, J=\text{even}, M\rangle$	A_1	$[K, J, M\rangle + (-1)^{-K} -K, J, M\rangle] / \sqrt{2}$
A_2	$ K=0, J=\text{odd}, M\rangle$	A_2	$[K, J, M\rangle - (-1)^{-K} -K, J, M\rangle] / \sqrt{2}$

^a Γ is the symmetry species in G_{36} (see Table 1 of [1]) to which the indicated rotational wavefunction belongs, using Euler angle transformations from Table 2 and transformation properties for symmetric top functions from [7].

order torsion and torsion–rotation terms that were not necessary for the ground state study of [3], but which are important for the many torsional levels studied here, have been added.

$$\begin{aligned}
 H = & A J_z^2 + B J_x^2 + C J_y^2 + F(p_1^2 + p_2^2) + 2F_{12}(p_1 p_2) + f(p_1^4 + p_2^4) \\
 & + f_{12}(p_1^2 p_2^2) + g_{12}(p_1 p_2)(p_1^2 + p_2^2) + \sum_{n>m} \sum_m [A_{mn}^{CC}(\cos 3m\alpha_1 \\
 & \times \cos 3n\alpha_2 + \cos 3n\alpha_1 \cos 3m\alpha_2) + A_{mn}^{SS}(\sin 3m\alpha_1 \sin 3n\alpha_2 \\
 & + \sin 3n\alpha_1 \sin 3m\alpha_2)] + \sum_m [A_{mm}^{CC}(\cos 3m\alpha_1 \cos 3m\alpha_2) \\
 & + A_{mm}^{SS}(\sin 3m\alpha_1 \sin 3m\alpha_2)] + (q + q_J J^2)(p_1 - p_2) J_z \\
 & + (r + r_J J^2)(p_1 - p_2) J_x + (A C J_z^2 + B C J_x^2 + C C J_y^2)(\cos 3\alpha_1 + \cos 3\alpha_2)
 \end{aligned} \quad (4)$$

This Hamiltonian consists of the three rigid-asymmetric-rotor operators, a pure torsional Hamiltonian similar to that given in [4], and a number of torsion–rotation terms allowed by the G_{36} symmetry group.

Matrix elements of the torsional and rotational operators in this Hamiltonian in the simple-product basis set $\exp(ik_1 \alpha_1) \exp(ik_2 \alpha_2) |K, J, M\rangle$ are well known, and will not be discussed further here. The Hamiltonian was partially block-diagonalized according to torsional symmetry species by restricting the k_1, k_2 torsional basis set quantum numbers to obtain four blocks, containing: A_1, A_2, A_3, A_4 species; E_1, E_2 species; E_3, E_4 species; and G species, as shown in Table 2 of [2]. Table 3 shows that multiplying the torsional basis functions by the rotational basis functions $|K, J, M\rangle$ does not destroy this symmetry-species grouping, since $A_2 \times \{A_1, A_2, A_3, A_4\} = \{A_2, A_1, A_4, A_3\}$, $A_2 \times \{E_1, E_2\} = \{E_1, E_2\}$, and $A_2 \times \{E_3, E_4\} = \{E_4, E_3\}$. Further factorization by symmetry would have required taking sums and differences of the basis functions, necessitating special treatment for matrix elements involving $K = 0, m = 0$, etc. This further factorization would have resulted in a factor of four decrease in the size of the Hamiltonian to be diagonalized for A species and a factor of two decrease in size for E species, but it was not implemented, since we preferred to sacrifice computational speed in order to reduce the possibility of introducing difficult-to-find errors involving minus signs and $\sqrt{2}$'s in the program code.

The Hamiltonian matrices for the $\tilde{A}^1 A_u$ state were set up with a maximum value of $k_1 = k_2 = 24$, and the matrix was diagonalized in a single step. As mentioned, this led to a very slow least-squares fitting process, so that a run of several iterations took several hours.

The torsion–rotation Hamiltonian operator for the $\tilde{X}^1 A_g$ (S_0) ground electronic state of biacetyl, where the torsional splittings are barely resolvable, was taken to be the sum of a rigid-rotor Hamiltonian and a constant torsional splitting depending only on the symmetry species Γ of the torsional sublevel:

$$H = A J_z^2 + B J_x^2 + C J_y^2 + T_0(\Gamma) - T_0(A_1) \quad (5)$$

where $\Gamma = A_1, G$, or (E_1, E_3) , as shown in Fig. 4 of [2].

4. Data set

The data set available here consists of about 180 transitions from our previously published rotational analyses [1] together with over 230 unpublished transitions. A brief summary of the rovibronic selection rules governing the observed transitions in the data set is as follows. Rovibronic (superscript etr = electronic-torsional-rotational) selection rules on the symmetry species Γ of the G_{36} permutation-inversion group appropriate for biacetyl require $etr \Gamma' \times etr \Gamma'' \supseteq A_3$. Since $e \Gamma' \times e \Gamma'' = A_3$ for a ${}^1 A_u - {}^1 A_g$ electronic transition in the C_{2h} frame, the G_{36} torsion–rotation selection rules become $etr \Gamma' \times etr \Gamma'' \supseteq A_1$. If the molecule-fixed axis system is kept locked to the non-hydrogenic frame of biacetyl, then the B_g in-plane and A_g out-of-plane C_{2h} direction cosines of the laboratory-fixed Z

Table 4

Rotational transitions used in the torsion–rotation analysis of the $\tilde{A}^1 A_u - \tilde{X}^1 A_g$ electronic transition of biacetyl.

Γ'	$(v'_1, v'_2)^a$	Range ^b	Γ''	$(v''_1, v''_2)^a$	Range ^b	v_0^c	Number ^d
$\tilde{A}^1 A_u$			$\tilde{X}^1 A_g$				
G	(0, 0)	$0 \leq J' \leq 4,$ $0 \leq K'_a \leq 3$	G	(0, 0)	$0 \leq J'' \leq 3,$ $0 \leq K''_a \leq 3$	22 178	37
E_1	(0, 0)	$0 \leq J' \leq 3,$ $0 \leq K'_a \leq 2$	E_1	(0, 0)	$0 \leq J'' \leq 3,$ $0 \leq K''_a \leq 2$	22 179	17
E_3	(1, 0)	$0 \leq J' \leq 3,$ $0 \leq K'_a \leq 2$	E_3	(0, 0)	$0 \leq J'' \leq 3,$ $0 \leq K''_a \leq 2$	22 265	25
G	(1, 0)	$0 \leq J' \leq 4,$ $0 \leq K'_a \leq 2$	G	(0, 0)	$0 \leq J'' \leq 3,$ $0 \leq K''_a \leq 2$	22 266	29
E_1	(1, 0)	$0 \leq J' \leq 3,$ $0 \leq K'_a \leq 2$	E_1	(0, 0)	$0 \leq J'' \leq 3,$ $0 \leq K''_a \leq 2$	22 275	33
G	(1, 0)	$0 \leq J' \leq 3,$ $0 \leq K'_a \leq 2$	G	(0, 0)	$0 \leq J'' \leq 3,$ $0 \leq K''_a \leq 1$	22 276	22
A_2	(1, 0)	$0 \leq J' \leq 3,$ $0 \leq K'_a \leq 2$	A_1	(0, 0)	$0 \leq J'' \leq 2,$ $0 \leq K''_a \leq 2$	22 278	13
A_1	(2, 0)	$0 \leq J' \leq 5,$ $0 \leq K'_a \leq 2$	A_1	(0, 0)	$0 \leq J'' \leq 5,$ $0 \leq K''_a \leq 2$	22 329	22
G	(2, 0)	$0 \leq J' \leq 4,$ $0 \leq K'_a \leq 3$	G	(0, 0)	$0 \leq J'' \leq 4,$ $0 \leq K''_a \leq 3$	22 330	40
E_1	(2, 0)	$0 \leq J' \leq 3,$ $0 \leq K'_a \leq 2$	E_1	(0, 0)	$1 \leq J'' \leq 3,$ $0 \leq K''_a \leq 2$	22 343	13
G	(2, 0)	$0 \leq J' \leq 4,$ $0 \leq K'_a \leq 3$	G	(0, 0)	$0 \leq J'' \leq 4,$ $0 \leq K''_a \leq 3$	22 344	43
E_3	(1, 1)	$0 \leq J' \leq 3,$ $0 \leq K'_a \leq 3$	E_3	(0, 0)	$0 \leq J'' \leq 3,$ $0 \leq K''_a \leq 2$	22 364	23
E_1	(1, 1)	$0 \leq J' \leq 4,$ $0 \leq K'_a \leq 1$	E_1	(0, 0)	$0 \leq J'' \leq 3,$ $0 \leq K''_a \leq 2$	22 364	17
G	(1, 1)	$0 \leq J' \leq 4,$ $0 \leq K'_a \leq 3$	G	(0, 0)	$0 \leq J'' \leq 3,$ $0 \leq K''_a \leq 2$	22 366	34
A_1	(1, 1)	$0 \leq J' \leq 4,$ $0 \leq K'_a \leq 2$	A_1	(0, 0)	$0 \leq J'' \leq 4,$ $0 \leq K''_a \leq 2$	22 367	28
G	(2, 1)	$0 \leq J' \leq 4,$ $0 \leq K'_a \leq 4$	G	(0, 0)	$0 \leq J'' \leq 3,$ $0 \leq K''_a \leq 3$	22 422	28
E_3	(2, 1)	$0 \leq J' \leq 3,$ $0 \leq K'_a \leq 3$	E_3	(0, 0)	$0 \leq J'' \leq 2,$ $0 \leq K''_a \leq 2$	22 434	16

^a Γ' and Γ'' are the torsional symmetry species of the upper and lower torsional states of the transition, respectively. Vibronic symmetries can be obtained by multiplying by the symmetry species of the electronic states: $\Gamma(\tilde{A}^1 A_u) = A_3$ and $\Gamma(\tilde{X}^1 A_g) = A_1$. The local mode quantum numbers for the upper and lower torsional states are given by v'_1, v'_2 and v''_1, v''_2 , respectively.

^b The range of upper and lower state rotational quantum numbers present in the fit.

^c These approximate band origins v_0 are illustrated in Figs. 1–3 and 5 of [2].

^d Number of rotational lines for this vibronic band used in the fit.

axis become A_2 (in-plane) and A_1 (out-of-plane) in G_{36} . Torsional selection rules then become ${}^t \Gamma' \times {}^t \Gamma'' \supseteq A_1$ or A_2 , so that allowed transitions from the four torsional tunneling components of the ground state populated in the cold jet become $({}^t A_1$ or ${}^t A_2) \leftarrow {}^t A_1$, ${}^t G \leftarrow {}^t G$, ${}^t E_1 \leftarrow {}^t E_1$, and $({}^t E_3$ or ${}^t E_4) \leftarrow {}^t E_3$. It is for this reason that torsional levels of species ${}^t A_3, {}^t A_4$, and ${}^t E_2$ have been removed from column 5 of Figs. 1–3 of [2]. (Note that the G_{36} symmetry labels in columns 4 and 5 of Figs. 1–3 of [2] are all ${}^t \Gamma$.)

Relative measurement precision of individual lines within a given laser scan is estimated to be 0.003 cm^{-1} , but there is some evidence that splicing the individual laser scans together can add another 0.002 cm^{-1} uncertainty when the data set is taken as a whole. Assignment of J', K' , and Γ' values for the transitions was greatly aided by requiring the quantum-beat patterns of transitions to the same upper state to be the same, though some judgment was required in deciding how dissimilar two patterns had to be to rule out the possibility that the corresponding transitions shared a common upper state. In this respect, the three pairs of identical quantum-beat patterns shown in [1] represent particularly unambiguous cases. The J, K, Γ and torsional distribution of our assigned lines and the approximate band centers of the vibronic transitions are shown in Table 4. The set of torsional energy levels in the excited electronic state for torsional excitations from zero

Table 5

The assignment and fitting status in this work of torsional levels of the $\tilde{A}^1A_u(S_1)$ state with four quanta or less of torsional excitation. (See Figs. 1–6 of [2] for a graphical display of these levels.)

ν^a	$\nu_1\nu_2^b$	Resolution ^c	Torsional components in G_{36}^d	Band origin regions ^e
4	22	Low	$A_1 G E_3 E_1$	
4	31⊕13	High/low	$[E_2] E_3 E_4 G E_1 [A_4] G A_1$	
4	40⊕04	High/low	$A_1 G [A_4] E_3 E_1 G [E_2] E_4$	
3	21⊕12	High	$[A_3] \{G\} A_2 [E_2] \{E_3\} G E_4 E_1$	22 423, 22 434, 22 445 cm^{-1}
3	30⊕03	Low/high	$[E_2] E_4 G E_3 E_1 [A_3] A_2 G$	22 390 and 22 443 cm^{-1}
2	11	High	$E_3 E_1 G A_1$	22 365 cm^{-1}
2	20⊕02	High	$A_1 G [A_4] (E_3) E_1 G [E_2] (E_4)$	22 329 and 22 343 cm^{-1}
1	10⊕01	High	$[E_2] E_3 G [A_3] E_1 (E_4) G A_2$	22 265 and 22 275 cm^{-1}
0	00	High	$(A_1) G (E_3) E_1$	22 178 cm^{-1}

^a The total number of torsional quanta excited, i.e., $\nu = \nu_1 + \nu_2$.

^b The local mode distribution of the torsional quanta.

^c Spectral resolution used to record transitions to the torsional components in that row.

^d Transitions to symmetry species in square brackets [] are forbidden at 1 K [2] and are not seen. For the rows with $\nu \leq 2$, transitions to symmetry species in parentheses () have not been found, presumably because they are weak; transitions to the 15 upper states without parentheses or brackets have all been rotationally analyzed. For the rows with $\nu \geq 3$, only transitions to the two 21⊕12 states in braces { } have been rotationally analyzed; other transitions with high resolution spectra had no quantum-beat information, which prevented reliable rotational assignments (particularly since their regions often involved many overlapping torsional bands).

^e Approximate wavenumber regions for band origins of transitions to torsional levels in this row.

to five quanta are illustrated in Figs. 1–6 of [2]. Table 5 lists the nine local-mode levels in these figures with four quanta of torsional excitation or less, together with all their torsional splitting components in G_{36} notation, and the level of spectral resolution and assignment status presently available for bands involving these levels in the $\tilde{A}^1A_u(S_1) - \tilde{X}^1A_g(S_0)$ electronic transition.

A number of different subsets of the full data set were used in the least-squares fits examined in this work. These subsets differed primarily in the number of torsional bands included. Three of these fits will be discussed below.

5. Least-squares fits

5.1. Parameter sets

As mentioned in connection with Eq. (5), five molecular constants were used to describe the lower state energy levels, namely

Table 6

Ground state molecular constants in cm^{-1} for the three fits discussed here.

Constant ^a	Fit 1 ^b	Fit 2 ^c	Fit 3 ^d
A	0.17711(15)	0.17718(14)	0.17695(18)
B	0.11236(15)	0.11238(13)	0.11232(16)
C	0.07039(18)	0.07032(16)	0.07052(20)
$(E_1, E_3) - A_1$	0.0352(22)	0.0330(21)	0.0533(19)
$G - A_1$	0.0122(18)	0.0102(16)	0.0316(14)

^a One standard uncertainty (type A, $k = 1$ [8]) is given in parentheses for the fitted molecular constants.

^b This fit included 415 transitions to 16 torsional states ($\nu = 1 E_3$ in Table 5, near 22 265 cm^{-1} was excluded) and 24 adjusted parameters, with an overall standard deviation of 0.0049 cm^{-1} .

^c This fit included 411 transitions to 16 torsional states ($\nu = 1 G$ in Table 5, near 22 266 cm^{-1} was excluded) and 24 adjusted parameters, with an overall standard deviation of 0.0045 cm^{-1} .

^d This fit included 440 transitions to 17 torsional states (all torsional states included) and 25 adjusted parameters, with an overall standard deviation of 0.0057 cm^{-1} .

the rotational constants A, B, and C in Eq. (4) and the small tunneling splittings $(E_1, E_3) - A_1$ and $G - A_1$ in the torsional ground state. Values for these constants obtained from the three least-squares fits discussed here are shown in Table 6. The rotational constants obtained for the ground state are essentially identical in the three fits. In the high-barrier limit, we expect the tunneling splittings to obey $[(E_1, E_3) - A_1] \approx 2[G - A_1]$, and this is satisfied for each fit to within a few standard uncertainties, although (somewhat surprisingly) corresponding splitting parameters differ by approximately a factor of two between the first two fits and the third.

In the first two fits described here, 19 molecular constants were used to describe the upper state rotational levels in 16 torsional states. The constants can be divided into 12 pure torsional constants, 3 pure rotational constants, 3 torsion–rotation interaction constants, and a band origin. The third fit differs from the first two by having rotational levels from one more torsional state included in the data set, and by using one less pure torsional constant and two more torsion–vibration constants.

The purely torsional constants from the three fits are given in Table 7, where corresponding values from the torsional fits in [2] and [4] are also noted.

Rotational constants in the upper state have nearly their usual asymmetric-rotor meanings, except that by setting all off-diagonal quadratic rotational constants to zero (i.e., by setting terms in $J_x J_z$ equal to zero) in Eq. (4), we have implicitly carried out a contact transformation to remove contributions from terms of that type which come from the torsion–rotation part of the two-top Hamiltonian [9]. This means that we are not in the usual moment-of-inertia principal axis system, but rather in what might loosely be called a “torsion–rotation principal axis system.” Torsion–rotation constants can be divided into those accounting for Coriolis interactions of angular momenta generated by internal rotation tunneling of the two methyl tops with the angular momentum of overall rotation, and those accounting for torsion–rotation changes of various pure rotational or pure torsional constants. Values for the rotation and torsion–rotation constants obtained from the present fits are given in Table 8.

The full least-squares fits are given in the Supplemental material, including the fitting program, and input and output files. Some difference in notation occurs between the text of this paper and the computer-generated materials; many of these differences are described in the accompanying readme file.

5.2. Discussion of the fits and fitting constants

The most perplexing problem in the present global fitting work is the fact that two different fits to rotational levels from 16 torsional states give a standard deviation near 0.005 cm^{-1} , but the standard deviation rises dramatically to 0.007 cm^{-1} when a similar fit of all 17 rotationally assigned torsional states is attempted. Only when a rather different set of parameters is chosen, can the standard deviation be brought down to 0.006 cm^{-1} .

Another way of looking at these fits is illustrated in Table 9, which can be used to draw some conclusions concerning the relative importance of measurement errors versus model errors in our fits. The columns headed “avg” in Table 9 give the average value in cm^{-1} of the signed observed-minus-calculated residuals multiplied by 10^3 . In a fit with no model errors and no calibration errors between different laser scans, these averages would be expected to lie very close to zero, deviating only by amounts comparable to the individual-line measurement error divided by the square root of the number of residuals in the average. Since this quantity is expected to be of the order of 0.001 cm^{-1} or less, it can be seen from the fits with only 16 torsional levels, that model or calibration errors of the order of 0.005 cm^{-1} remain. The contribution of calibration errors can be estimated by looking at the averages for

Table 7
Upper state pure torsional constants^a in cm⁻¹ obtained from the present least-squares fits.

Constant ^a	Fit 1 ^b	Fit 2 ^b	Fit 3 ^b	Ref. [2]	Ref. [4]
<i>F</i>	5.2467(27)	5.2510(25)	5.2532(31)	5.3543(85)	5.5885
<i>F</i> ₁₂	0.0649(17)	0.0612(15)		-0.237(33)	-0.2522
<i>f</i>	-0.00161(18)	-0.00178(16)	+0.00174(12)		
<i>f</i> ₁₂	0.00076(16)	0.00074(15)			
<i>g</i> ₁₂			0.00459(28)		
<i>A</i> ₀₀ ^{CC}	<i>v</i> ₀ ^a	<i>v</i> ₀ ^a	<i>v</i> ₀ ^a	136.34(22)	227.29
<i>A</i> ₀₁ ^{CC}	116.553(50)	116.497(46)	119.147(52)	122.68(14)	116.57
<i>A</i> ₀₂ ^{CC}	-6.31(19)	-6.44(17)			-1.97
<i>A</i> ₀₃ ^{CC}	-2.70(27)	-2.92(25)	9.899(37)		
<i>A</i> ₀₄ ^{CC}	-1.15(21)	-1.35(19)	14.407(88)		
<i>A</i> ₁₁ ^{CC}	6.870(61)	6.772(56)	7.435(65)	15.14(19)	0.14
<i>A</i> ₁₁ ^{SS}	-21.17(12)	-21.09(11)	-22.54(23)	-12.3(14)	-9.00
<i>A</i> ₁₂ ^{CC}	0.424(37)	0.345(34)		4.068(76)	-3.93
<i>A</i> ₁₂ ^{SS}	-0.942(36)	-0.922(34)	-2.773(87)	-1.25(22)	
<i>A</i> ₂₂ ^{CC}			-0.816(21)		1.78
<i>A</i> ₂₂ ^{SS}			-1.952(46)		
$\sigma \times 10^3$	4.9	4.5	5.7		

^a From the Hamiltonian operator in Eq. (4), *F* is the effective rotational constant of the two equivalent tops, and *F*₁₂ is the quadratic top-top kinetic-energy interaction term; *f*, *f*₁₂, *g*₁₂ are quartic torsional centrifugal distortion constants. *A*₀₀^{CC} in Refs. [2] and [4] is a potential energy offset of little physical significance; it is replaced in fits 1, 2, and 3 here by the band origins *v*₀ = 22 313.683(32), 22 313.643(30), and 22 314.320(37). The quantities 2 *A*₀₁^{CC}, 2*A*₀₂^{CC}, 2*A*₀₃^{CC}, and 2*A*₀₄^{CC} are the usual *V*₃, *V*₆, *V*₉, and *V*₁₂ barrier-height Fourier expansion coefficients for the two equivalent tops in biacetyl. *A*₁₁^{CC} and *A*₁₁^{SS} are threefold top-top cosine and sine potential interaction terms; *A*₁₂^{CC} and *A*₁₂^{SS} are mixed threefold-sixfold top-top interaction terms; *A*₂₂^{CC} and *A*₂₂^{SS} are sixfold top-top cosine and sine potential interaction terms. One standard uncertainty (type A, *k* = 1 [8]) is given in parentheses for the fitted parameters.

^b Fits 1, 2, and 3 are as described in the footnotes of Table 6.

torsional bands with nearly the same band origin, since such bands normally are measured in the same laser scan. Comparison of avg values in fit 1 for the overlapping *A*₁ and *G* torsional bands near 22 277 cm⁻¹ indicates that the oppositely signed magnitudes of -0.0036 and +0.0044 cm⁻¹ cannot be explained by calibration errors, and must therefore arise from model errors.

The columns headed “rms” give the root-mean-square of (obs - calc - avg) values in cm⁻¹ multiplied by 10³, which measure the distribution of (obs - calc) values about avg and not about zero. In a fit with little or no rotational model error, these rms values would be expected to lie very close to the expected individual-line measurement precision of 0.003 cm⁻¹ or so. This is indeed the case for many of the torsional bands, and in particular, it is the case for the 25 transitions in the *E*₃ torsional level excluded from fit 1 in Table 9, leading us to conclude that the biggest source of error in our fits is from unknown error(s) in our modeling of the torsional band origins. We have tried adding additional terms to the purely torsional part of the Hamiltonian, but without much success. Since the errors under discussion here are of the order of 0.04 cm⁻¹ when one torsional state is excluded (fits 1 and 2) or of the order of 0.01 cm⁻¹ when all 17 torsional states are fit together (fit 3), and since these errors occur in an excited electronic state, the possibility of random vibrational perturbations from unseen dark states cannot be eliminated.

Table 8
Pure rotation and torsion-rotation molecular parameters^a in cm⁻¹ obtained from the present fits^b.

Parameters ^a	Fit 1 ^b	Fit 2 ^b	Fit 3 ^b
<i>A</i>	0.18036(13)	0.18047(12)	0.18048(14)
<i>B</i>	0.11650(24)	0.11644(22)	0.11639(28)
<i>C</i>	0.07018(19)	0.07020(17)	0.07029(22)
<i>q</i>	-0.23326(66)	-0.23322(61)	-0.2354(18)
<i>q</i> _{<i>J</i>}			-0.00087(15)
<i>r</i>	0.13726(72)	0.13732(66)	0.1496(25)
<i>r</i> _{<i>J</i>}			-0.00080(21)
<i>B</i> _{<i>C</i>}	0.00128(24)	0.00106(23)	0.00104(28)

^a The parameters *q* and *r* describe first-order torsion-rotation Coriolis interaction about the *z* and *x* axes, respectively. One standard uncertainty (type A, *k* = 1 [8]) is given in parentheses for the parameters.

^b Fits 1, 2, and 3 are as described in the footnotes of Table 6.

A second question concerns the stability of the model parameters as the number of states included in the fit is increased. Table 6 indicates that the ground state rotational constants are stable to within their standard uncertainties, when fits 1, 2, and 3 are

Table 9

Summary of two fits involving rotational transitions to 16 torsional levels and one fit involving rotational transitions to 17 torsional levels^a.

Torsional state			Fit 1 ^a		Fit 2 ^a		Fit 3 ^a		
	<i>J</i> ^b	<i>v</i> ^c	num ^d	avg ^e	rms ^f	avg ^e	rms ^f	avg ^e	rms ^f
<i>A</i> ₂		22 278	13	-3.6	1.7	-3.2	1.9	-7.8	1.5
<i>A</i> ₁		22 329	22	0.7	2.7	0.4	2.5	1.3	2.9
<i>A</i> ₁		22 367	28	1.1	3.1	1.2	3.3	2.6	3.4
<i>E</i> ₁		22 179	17	-0.7	2.4	-1.0	2.2	-0.2	2.3
<i>E</i> ₁		22 275	33	-1.5	4.3	-1.4	4.3	-1.9	3.5
<i>E</i> ₁		22 343	13	0.7	3.9	0.8	4.0	1.6	4.5
<i>E</i> ₁		22 364	17	5.2	4.1	4.4	4.2	10.1	3.1
<i>E</i> ₃		22 265	25	-40.3*	1.9	0.1	1.9	-2.9	2.0
<i>E</i> ₃		22 364	23	-1.6	4.0	-1.1	4.2	-2.5	3.2
<i>E</i> ₃		22 434	16	0.1	7.5	0.1	7.6	0.1	10.1
<i>G</i>		22 178	37	0.2	3.4	0.4	3.1	-0.2	3.7
<i>G</i>		22 266	29	0.1	6.7	39.1*	7.3	2.7	5.5
<i>G</i>		22 276	22	4.4	3.4	4.1	3.5	7.7	3.3
<i>G</i>		22 330	40	-0.3	3.3	-0.1	3.2	-0.7	4.0
<i>G</i>		22 344	43	-0.3	7.2	-0.3	7.0	-0.6	6.3
<i>G</i>		22 366	34	-2.5	2.6	-2.5	2.8	-5.6	2.2
<i>G</i>		22 422	28	0.0	4.2	0.0	4.3	-0.1	5.2
Number of parameters					24		24		25
Number of transitions						415		411	440
Overall rms of the fit						4.9		4.5	5.7

^a These fits are as indicated in the footnotes to Table 6. The torsional level removed from Fits 1 and 2 is indicated by an *.

^b The symmetry of the torsional level in *G*₃₆.

^c The approximate position of the torsional level in cm⁻¹.

^d Number of rotational transitions to that torsional level used in the fit.

^e Average in cm⁻¹ of the signed values of (obs - calc) × 10³. In a perfect fit, this average would fluctuate about zero with an amplitude ≈ (measurement error)/√num ≈ ±0.001 cm⁻¹.

^f rms in cm⁻¹ of the quantity (obs - calc - avg) × 10³, which gives a measure of assignment and measurement errors within a given sub-band, after torsional model errors have been removed.

compared. From a relative point of view, the torsional splittings of the ground state differ by a factor of two among these three fits. From an absolute point of view, however, they differ by only 0.02 cm^{-1} , which is comparable to the 0.04 cm^{-1} deviations of, for example, the excluded E_3 state near 22265 cm^{-1} in fit 1 of Table 9. We suppose that these 0.04 cm^{-1} deviations are somehow redistributed when this E_3 state is included (in fit 3), which may account for the large (and therefore possibly spurious) change in the ground state splitting parameters when the larger data set is treated. Unfortunately, biacetyl has no permanent dipole moment, so traditional microwave studies to determine accurate ground state rotational constants and torsional splittings are not possible. Nevertheless, there may be some hope that the π -electrons in the two carbonyl bonds could assist in generating a rotationally induced dipole moment large enough for studies like those carried out on BF_3 [10], C_3H_6 (cyclopropane) [11], and SO_3 [12], but the authors have not attempted any calculations concerning this question.

Table 7 indicates that apart from F and V_3 , the purely torsional parameters (including the important top–top interaction terms in the kinetic and potential energy) are not at all stable when the torsional levels in the fit are increased in passing from Ref. [4] to [2] to the present fits. This could again indicate some deficiency in the present two-top torsional model, or it could be a reflection of small perturbations from dark levels of the ground electronic state or the first excited triplet state that may lie nearby. The change in F_{12} , which varies from positive to indeterminate to negative across the five fits shown in Table 7, is particularly striking, and precludes using the pure torsional constants to get physically meaningful structural information on the excited electronic state.

On the other hand, Table 8 indicates that the pure rotational and the torsion–rotation constants in the upper state are quite stable across the three fits of rotational transitions discussed here. The ratio of q/r is consistent (using a simple one top model) with an angle between the methyl top and the principal a axis somewhere in the vicinity of 40° to 45° .

In conclusion, we believe that our line assignments and the upper and lower state rotational constants determined from them are correct. We have no confirmed explanation for our difficulties (at the 0.01 cm^{-1} level) in fitting all 17 torsional levels. This inability to accurately fit the torsional levels also prevented us from making rotational line assignments based on energy level calcula-

tions extrapolated to the higher energy (and spectrally denser) regions where rotationally resolved spectra were recorded (see Figs. 3 and 5 of [2]), but where no quantum-beat information (needed to confirm transitions to the same upper state) was available.

As a final comparison, we note that the ab initio value for the magnitude of the ground state (S_0) barrier in biacetyl [4] is $V_3 = 338\text{ cm}^{-1}$, which can be compared with the microwave value for the ground state barrier in methyl glyoxal [13] of $V_3 = 269\text{ cm}^{-1}$. Fits 1–3 in Table 7 here give upper state barrier estimates in the range from 233 to 238 cm^{-1} .

Appendix A. Supplementary data

Supplementary data for this article are available on ScienceDirect (www.sciencedirect.com) and as part of the Ohio State University Molecular Spectroscopy Archives (http://library.osu.edu/sites/msa/jmsa_hp.htm). Supplementary data for this article consist of a readme file, the least-squares program, input and output files for fits 1, 2, and 3 presented in part in Tables 6–9, and one file showing the execution commands for fit 1.

References

- [1] C.-L. Huang, H.-H. Liu, C.-L. Liu, A.H. Kung, C.-K. Ni, J. Chem. Phys. 117 (2002) 5165–5173.
- [2] C.-L. Huang, C.-L. Liu, C.-K. Ni, J.T. Hougen, J. Mol. Spectrosc. 233 (2005) 122–132.
- [3] N. Ohashi, J.T. Hougen, R.D. Suenram, F.J. Lovas, Y. Kawashima, M. Fujitake, J. Pyka, J. Mol. Spectrosc. 227 (2004) 28–42.
- [4] M.L. Senent, D.C. Moule, Y.G. Smeyers, A. Toro-Labbé, F.J. Peqalver, J. Mol. Spectrosc. 164 (1994) 66–78.
- [5] D.D. Nelson Jr., W. Klemperer, J. Chem. Phys. 87 (1987) 139–149.
- [6] E.B. Wilson Jr., J.C. Decius, P.C. Cross, Molecular Vibrations, McGraw–Hill, New York, 1955.
- [7] J.T. Hougen, J. Chem. Phys. 37 (1962) 1433–1441.
- [8] Guidelines for Evaluating and Expressing the Uncertainty of NIST Measurement Results, NIST Technical Note 1297, 1994. Available from: <<http://physics.nist.gov/cuu/Uncertainty/index.html>>.
- [9] J.E. Wollrab, Rotational Spectra and Molecular Structure, Academic Press, New York, 1967.
- [10] M. Oldani, A. Bauder, J. Chem. Phys. 86 (1987) 624–628.
- [11] Th. Brupbacher, Ch. Styger, B. Vogelsanger, I. Ozier, A. Bauder, J. Mol. Spectrosc. 138 (1989) 197–203.
- [12] V. Meyer, D.H. Sutter, H. Dreizler, Z. Naturforsch. A46 (1991) 710–714.
- [13] C.E. Dyllick-Brenzinger, A. Bauder, Chem. Phys. 30 (1978) 147–153.